JOURNAL OF GEOPHYSICAL RESEARCH, VOL. 113, B01102, doi:10.1029/2007JB005132, 2008

Click Here for Full Article

Response of submarine hydrologic monitoring instruments to formation pressure changes: Theory and application to Nankai advanced CORKs

Audrey Hucks Sawyer,[1,2] Peter Flemings,[1,2] Derek Elsworth,[3] and Masataka Kinoshita[4]

Received 24 April 2007; revised 6 August 2007; accepted 28 September 2007; published 18 January 2008.

[1] We describe the response of a compressible submarine hydrologic monitoring instrument to formation pressure changes in low-diffusivity rock. The measured pressure depends on the frequency of the pressure signal, the hydraulic diffusivity, and the wellbore storage. The Nankai advanced circulation obviation retrofit kits (ACORKs) (offshore Japan) record tide-induced formation pressure changes with small amplitudes (<10% of seafloor amplitudes) and large phase shifts (>25°). The pressure measurements occur in thick, homogeneous, compressible, low-permeability sediment, where in situ tidal pressure responses should approximate the seafloor tidal signal. A wellbore storage of 2×10^{-8} m^3 Pa^{-1} can explain many of the observed tidal responses, given the hydraulic diffusivities of the monitored intervals. A reduced permeability around the wellbore of 1000-fold and a wellbore storage of 10^{-11} m^3 Pa^{-1} can also reconcile the data. Our analysis suggests that ACORK screens in the Lower Shikoku Basin facies have a critical frequency on the order of 5×10^{-8} Hz (equivalent to a period of 250 days); higher-frequency formation pressure signals will be distorted in the pressure record. Within the Lower Shikoku Basin facies the time for this monitoring system to record 90% of an instantaneous pressure change is on the order of 10 d. We suggest that the ACORK instrument compliance contributes to, but does not fully explain, the small tidal amplitudes and large phase shifts recorded at the least permeable monitoring intervals.

Citation: Sawyer, A. H., P. Flemings, D. Elsworth, and M. Kinoshita (2008), Response of submarine hydrologic monitoring instruments to formation pressure changes: Theory and application to Nankai advanced CORKs, *J. Geophys. Res.*, *113*, B01102, doi:10.1029/2007JB005132.

1. Introduction

[2] Borehole monitoring of formation pressure changes requires that pressure in the instrument equilibrate with pressure in the formation. Consequently, large or compressible instruments filter formation pressure signals if the hydraulic diffusivity of the formation is sufficiently small. If formation pressure changes abruptly, the measured pressure asymptotically approaches the new formation pressure with time. If formation pressure oscillates with sufficiently high frequency, the measured pressure oscillation has a diminished amplitude and lags formation pressure. Numerous authors have presented this problem in open boreholes for both step [*Gibson*, 1963; *Cooper et al.*, 1967; *Papadopulos et al.*, 1973; *Bredehoeft and Papadopulos*, 1980] and cyclic [*Cooper et al.*, 1965; *Bredehoeft*, 1967; *Hsieh et al.*, 1987] pore pressure changes.

[3] Circulation obviation retrofit kits (CORKs) have monitored pressures in tectonically active submarine settings for over a decade [*Davis and Becker*, 2001]. CORKs in the Barbados accretionary prism penetrate the décollement and record overpressures that are 30% to 60% of hydrostatic effective stress (the difference between hydrostatic and lithostatic pressure) [*Becker et al.*, 1997; *Foucher et al.*, 1997]. Barbados CORK data also indicate that décollement permeability is greater than surrounding sediment permeability [*Screaton et al.*, 2000]. *Davis et al.* [2006] described abrupt pressure transients at Nankai Trough advanced CORKs (ACORKs) (offshore Japan), and suggested they represent earthquake-induced strain. In the Costa Rica prism, CORKs recorded transient pressure and temperature signals approximately two weeks after the onset of onshore strain events detected by a GPS network [*Davis and Villinger*, 2006]. CORKs in the Juan de Fuca Ridge recorded several pressure transients associated with seafloor spreading events [*Davis et al.*, 2001, 2004].

[4] In these studies, the measured pore pressure was assumed to equal the in situ pressure. Notably, recorded tidal pressure responses often had amplitude attenuations

[1]Department of Geosciences, Pennsylvania State University, University Park, Pennsylvania, USA.
[2]Now at the Department of Geological Sciences, University of Texas at Austin, Austin, Texas, USA.
[3]Department of Energy and Mineral Engineering, Pennsylvania State University, University Park, Pennsylvania, USA.
[4]Institute for Research on Earth Evolution, Japan Agency for Marine-Earth Science and Technology, Kanagawa, Japan.

Copyright 2008 by the American Geophysical Union.
0148-0227/08/2007JB005132$09.00

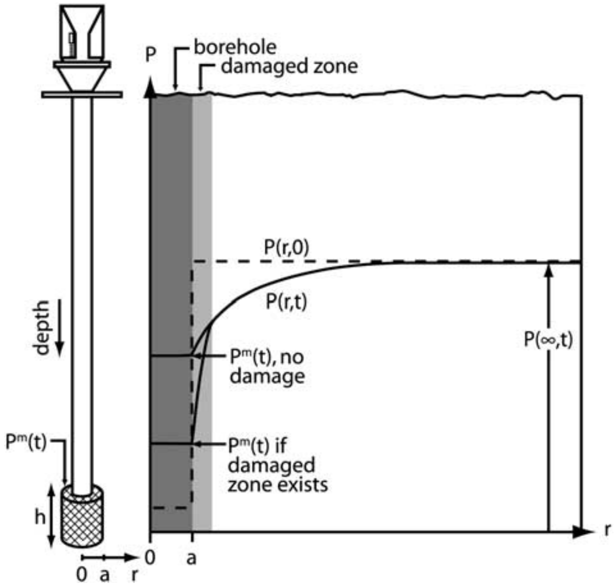

Figure 1. (left) Sketch of monitoring system. Screens of height h measure pressure, $P^m(t)$, at the screen radius. (right) Pressure response to an initially offset formation pressure, $P(r, 0)$ (dashed line). Dark shading indicates the borehole and screen region ($r < a$). The measured pressure, $P^m(t)$, equilibrates with the formation pressure, $P(\infty, t)$, as fluid flows to the screen (solid line, no damaged zone). A zone of reduced permeability around the borehole (light shading, damaged zone) increases the pressure gradient near the screen and impedes pressure equilibration.

and phase shifts relative to tidal pressure changes at the seafloor. For example, at the Juan de Fuca Ridge, tidal amplitudes in the basement approach 28% of seafloor amplitudes and lag the seafloor signal by as much as 20°. *Davis et al.* [2000] interpreted this tidal response to include a diffusive pressure signal that propagates from over 16 km away, where the basement outcrops at the seafloor. They also observed that positive phase shifts exceed predictions from vertical tidal loading models. In the Cascadia accretionary prism, the measured tidal pressure response leads the seafloor signal by several degrees and is attenuated to 55% of the seafloor response; *Wang and Davis* [1996] interpreted the existence of a gas-bearing layer below the BSR.

[5] At the Nankai ACORKs (offshore Japan), tidal signals have amplitudes as low as 10% of seafloor amplitudes and phase shifts of more than 25°. These tidal responses occur in thick, homogeneous, compressible, low-permeability sediments, where in situ pressure signals should have amplitudes greater than 90% of seafloor amplitudes. We review the response of a compressible instrument to high-frequency formation pressure changes. We then present the Nankai ACORK data as a case study. We show that if the ACORK wellbore storage factor is approximately 2×10^{-8} m^3 Pa^{-1}, the instrument is sufficiently compressible and voluminous to explain many of the observed tidal responses, given our estimates of hydraulic diffusivity. Alternatively, a small wellbore storage of 10^{-11} m^3 Pa^{-1} and a reduced permeability around the wellbore of 1000-fold can also reconcile the data. Ultimately, the ACORK wellbore storage is too large to permit accurate measurement of in situ pressures at tidal frequencies in hemipelagic mud. Actions to improve pressure monitoring may include designing stiffer instruments with smaller volumes, conducting well tests, and increasing permeabilities near screens through the use of sand packs, hydraulic fractures, or conventional well development.

2. Instrument Response to Formation Pressure Changes

[6] Consider a well, represented by a closed cylinder with screen radius $r = a$, surrounded by an infinite homogeneous medium (Figure 1). Formation fluid enters the well through the cylindrical screen. The nondimensionalized cylindrical flow equation describes pressure in the formation:

$$\frac{\partial^2 P_D}{\partial r_D^2} + \frac{1}{r_D}\frac{\partial P_D}{\partial r_D} + S_D(t_D) = \frac{\partial P_D}{\partial t_D}, \tag{1a}$$

where P_D is dimensionless pressure,

$$P_D = \frac{P(r,t)}{P(\infty,t)}. \tag{1b}$$

$P(\infty, t)$ is the formation pressure far from the well's sphere of influence; r_D is the dimensionless radius,

$$r_D = \frac{r}{a}, \tag{1c}$$

where a is the screen radius; t_D is dimensionless time,

$$t_D = \frac{ct}{a^2}, \tag{1d}$$

where c is the hydraulic diffusivity:

$$c = \frac{k}{\mu S_s}. \tag{1e}$$

k is intrinsic permeability, μ is fluid viscosity, and S_s is specific storage, given by

$$S_s = \rho g(m_v + n\beta_w). \tag{1f}$$

ρg is specific weight of the pore fluid, m_v is formation compressibility, n is porosity, and β_w is the compressibility of the pore fluid (Table 1). S_D (equation (1a) is a nondimensionalized time-varying fluid source term. Fluid volume is conserved between the formation and the well such that

$$\frac{\partial P_D^m}{\partial t_D} = \beta_D \frac{\partial P_D}{\partial r_D} \quad at \quad r_D = 1, \tag{2a}$$

where P_D^m is dimensionless pressure measured at the screen, normalized according to equation (1b), and β_D is the dimensionless formation-instrument compliance ratio:

$$\beta_D = \frac{2\pi a^2 h m_v}{\beta^* V}. \tag{2b}$$

Table 1. Symbols, Definitions, and Dimensions of Variables

Variable	Definition	Dimension
A	amplitude	-
a	screen radius	L
c	hydraulic diffusivity	$L^2\ t^{-1}$
E	imaginary pressure response parameter	-
F	imaginary pressure response parameter	-
h	screen height	L
k	intrinsic permeability	L^2
L	characteristic diffusion length	L
L_t	tubing length	L
m_v	formation compressibility	$M^{-1}\ L\ t^2$
n	porosity	-
$P(r, t)$	pressure	$M\ L^{-1}\ t^{-2}$
P_D^m	dimensionless measured pressure	-
P_D	dimensionless pressure	-
r	radius	L
r_D	dimensionless radius	-
r_{c_i}	casing inner radius	L
r_{c_o}	casing outer radius	L
r_{s_i}	screen inner radius	L
r_{s_o}	screen outer radius	L
r_{t_i}	tubing inner radius	L
r_{t_o}	tubing outer radius	L
S_D	dimensionless source term	-
S_s	specific storage	L^{-1}
T	temperature	°C
t	time	t
t_D	dimensionless time	-
V	system volume	L^3
β_D	formation-instrument compliance ratio	-
β_{steel}	steel compressibility	$M^{-1}\ L\ t^2$
β_w	fluid compressibility	$M^{-1}\ L\ t^2$
$\beta*$	system compressibility	$M^{-1}\ L\ t^2$
ε	fractional equilibration	-
γ	loading efficiency	-
μ	fluid viscosity	$M\ L^{-1}\ t^{-1}$
Φ	imaginary pressure response parameter	-
φ	phase	degrees
ρg	specific weight	$M\ L^{-2}\ t^{-2}$
Ψ	imaginary pressure response parameter	-
υ	Poisson's ratio	-
ω	radian frequency	t^{-1}
ω_D	dimensionless radian frequency	-

h is the cylindrical cavity height, $\beta*$ is the composite fluid and instrument compressibility, and V is instrument volume (Figure 1 and Table 1). Equation (2b) assumes the specific storage approximates the product of formation compressibility and specific weight of the fluid, which is common for sediment. Small values of β_D represent a more compressible instrument relative to the formation. The fluid pressure in the instrument (P_D^m) equals the formation pressure at the screen radius:

$$P_D^m = P_D \quad at \quad r_D = 1 \quad for \quad t_D > 0. \tag{3}$$

We first consider the case without a source term ($S_D = 0$), where pressure is initially uniform in the formation, and pressure in the borehole instantaneously decreases by ΔP at time zero (Figure 1, dashed line). Formation pressure is constant far from the borehole:

$$P_D \to 1 \quad as \quad r_D \to \infty \; for \quad t_D > 0. \tag{4}$$

[7] *Gibson* [1963] and *Bredehoeft and Papadopulos* [1980] solved this problem in spherical coordinates and cylindrical coordinates, respectively. β_D (equation (2b)) is equivalent to 2α in the *Neuzil* [1982] correction to the *Bredehoeft and Papadopulos* [1980] solution. We plot pressure equilibration (ε) versus the combined parameter $\beta_D t_D$ for different formation-instrument compliance ratios using *Bredehoeft and Papadopulos*' [1980] solution (Figure 2).

$$\varepsilon = \frac{P(\infty) - P(t)}{P(\infty) - P(0)} \tag{5}$$

For a given formation-instrument compliance ratio (β_D), equilibration increases with time or hydraulic diffusivity (Figure 2 and equation (1d)). With increasing β_D, equilibration occurs more rapidly (Figure 2 and equation (2b)).

[8] To consider sinusoidal changes in formation pressure, we include a uniform, time-varying source term (S_D) in equation (1a):

$$S_D(t_D) = \omega_D \cos(\omega_D t_D). \tag{6a}$$

ω_D is the nondimensionalized radian frequency (ω):

$$\omega_D = \frac{a^2 \omega}{c}. \tag{6b}$$

The inner boundary condition is unchanged, and we assign a no-flow outer boundary:

$$\frac{\partial P}{\partial r} \to 0 \quad as \quad r \to \infty. \tag{7}$$

Hsieh et al. [1987] solved this problem for head change in an open well due to Earth tide dilation of the surrounding confined aquifer. We modify their solution to describe pressure in a closed monitoring instrument. A, the measured amplitude in the instrument relative to amplitude in the far field, and ϕ, the phase shift, are given by

$$A = \frac{1}{\sqrt{E^2 + F^2}}, \tag{8a}$$

$$\phi = -\tan\left(\frac{E}{F}\right). \tag{8b}$$

E and F are defined in Appendix A.

[9] The measured pressure is a function of two dimensionless parameters: β_D, the formation-instrument compliance ratio (equation (2b)), and ω_D, the dimensionless frequency (equation (6b)) (Figures 3a and 3b). An instrument with low compressibility relative to the formation (high β_D) records pressure signals with negligible amplitude attenuations and phase shifts ($A \sim 100\%$, $\phi \sim 0$) over a wide range of frequencies (e.g., $\beta_D = 100$, Figures 3a and 3b). However, all instruments have some frequency threshold above which measured pressures depart from formation pressures. We define the critical frequency for a given β_D as the frequency where $A = 90\%$. For example, an instrument with $\beta_D = 100$ has a critical dimensionless frequency of 250

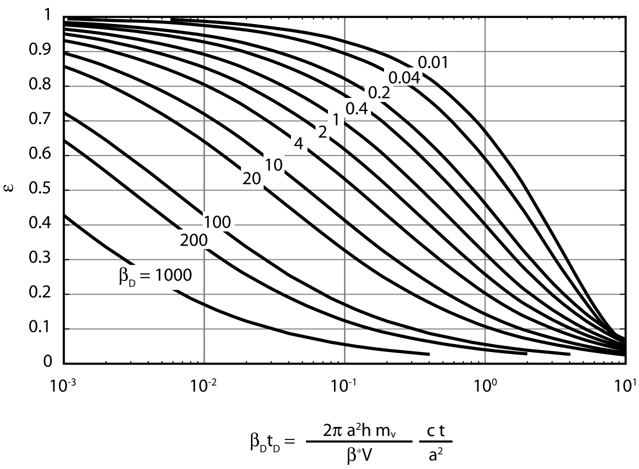

Figure 2. Equilibration of measured pressure with formation pressure in response to an instantaneous pressure offset plotted against combined parameter $\beta_D t_D$ [after *Bredehoeft and Papadopulos*, 1980]. Here $\varepsilon = 1$ represents no pressure equilibration between instrument and formation, and $\varepsilon = 0$ represents total equilibration. Smaller β_D values represent more compressible, voluminous instruments, and corresponding type curves have longer equilibration times.

(Figure 3a). Above this frequency, amplitude attenuation and phase shift of the measured signal increase rapidly. More compliant instruments (lower β_D) have lower critical frequencies.

3. A Case Study: Nankai ACORKs

[10] We use our model to analyze the fidelity of pressure measurements at two long-term hydrologic observatories (ACORKs) installed offshore of Japan in the Nankai Trough in June 2001 [*Mikada et al.*, 2002; *Davis et al.*, 2006] (Figure 4). The Nankai Trough marks the shallow subduction of the Philippine Sea Plate beneath the Eurasian Plate (Figure 4). The plate boundary (décollement) separates offscraped and accreted sediment of the Nankai accretionary prism from underthrust sediment and basement [*Taira et al.*, 1991] (Figure 5). At Ocean Drilling Program (ODP) Site 1173, the 16 Ma basement is successively overlain by volcaniclastics, a middle Miocene to mid-Pliocene hemipelagic mud (Lower Shikoku Basin facies), an upper Pliocene to lower Pleistocene hemipelagic mud with tephra layers (Upper Shikoku Basin facies), and a sequence of Pleistocene to Holocene interbedded turbidites and hemipelagic muds (Trench-Basin facies and Outer-Trench Wedge facies) [*Mikada et al.*, 2002] (Figure 6).

[11] ODP Site 808 penetrates the frontal thrust of the imbricate thrust zone and the décollement (Figure 5). The basaltic basement at ODP Site 808 is overlain by volcaniclastics, the Lower Shikoku Basin facies, Upper Shikoku Basin facies, Trench-Basin facies, and Outer Marginal Trench-Wedge facies (Figure 7). The stratigraphy at ODP Site 808 includes additional Pleistocene to Holocene sand and silt turbidite units not present at ODP Site 1173: Lower Axial Trench facies (thin-bedded sand and silt turbidites), Upper Axial Trench facies (thick-bedded sand turbidites), and Lower Slope facies (a thin, Quaternary hemipelagic

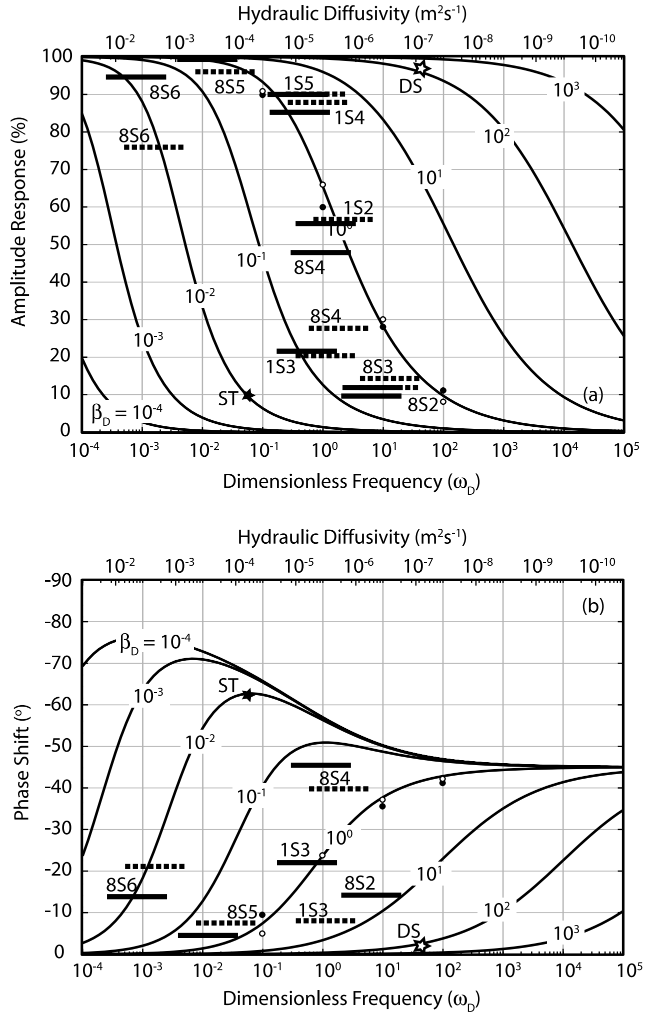

Figure 3. (a) Amplitude of measured pressure as a percentage of amplitude in the formation versus dimensionless frequency, ω_D (equation (6b)). The top axis indicates equivalent hydraulic diffusivity for each dimensionless frequency given a semidiurnal tidal frequency and ACORK screen radius (a = 0.156 m). More compliant instruments (lower β_D) record smaller amplitudes at a given frequency. For a given instrument (β_D), higher frequencies and lower diffusivities have smaller amplitude responses. (b) Phase of measured pressure with respect to formation pressure versus dimensionless frequency, ω_D (equation (6b)). Measured pressures increasingly lag formation pressures at higher frequencies and lower diffusivities. For a given instrument, higher frequencies result in greater phase lags. Horizontal bars indicate tidal responses for ODP Sites 808 and 1173 (solid bars indicate diurnal signals, and dashed bars indicate semidiurnal). Open stars show the predicted semidiurnal tidal response at ODP Site 808 screen 2 based on our β_D estimate from ACORK design specifications (DS). Solid stars show the same prediction based on our slug test (ST) analysis. Open and solid circles show the modeled instrument response for equivalent cylindrical and spherical screens, respectively. The cylindrical screen height is 25 times its radius, but the spherical screen with the same surface area has a nearly identical pressure response.

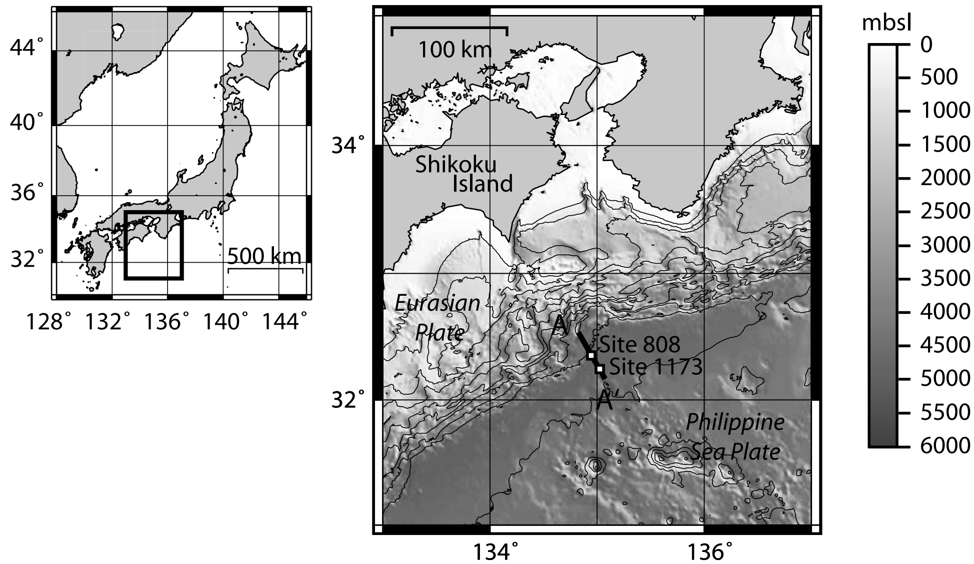

Figure 4. Bathymetry of the Nankai region in meters below seafloor (Japanese Agency for Marine Technology SeaBeam data) and ACORK locations. ODP Site 1173 is installed in the Nankai Trough, and ODP Site 808 penetrates the toe of the accretionary wedge. Schematic cross section A-A′ is shown in Figure 5.

mud and turbidite unit) (Figure 7). The frontal thrust at ODP Site 808 displaces the Outer Marginal Trench-Wedge facies over the Lower Axial Trench facies [*Mikada et al.*, 2002]. The Lower Shikoku Basin facies contains the décollement (Figure 7).

3.1. ACORK Design

[12] Each ACORK consists of a 10.75″ outside-diameter casing string with packers and monitoring screens suspended around it (Figures 6 and 7). A multiline hydraulic umbilical transmits screen pressures to sensors and data loggers at the seafloor. The hydraulic umbilical runs the length of the installation between the casing and borehole wall and passes successively through packers [*Becker and Davis*, 2005] (Figure 8). The inflatable packers consist of 3-m-long steel-reinforced rubber bladders. The screens, numbered sequentially from deepest to shallowest, are 7.6 m long and extend outward from the casing by 2 cm [*Becker and Davis*, 2005] (Figure 8). Because pressure sensors are located at the seafloor, the measurements for each screen share the same hydrostatic reference. Pumping valves, used for conducting well tests, are also located at the seafloor [*Becker and Davis*, 2005].

[13] The ACORKs represent a fundamental design change from previous CORK installations [*Becker and Davis*, 2005]. CORKs are cased holes with a single seal at the seafloor. Pressure monitoring occurs at the CORK head. The original CORKs integrate pressure over the length of open borehole or perforated interval. They do not measure pressure in multiple isolated zones, and they have no tubing to connect the open hole with gauges at the seafloor [*Becker and Davis*, 2005].

[14] The ACORK at ODP Site 1173 monitors pressures at five screens (Figure 8). A packer exists above each screen except screen 5 (Figure 6). A bridge plug, or hydraulic seal, was installed inside the casing to prevent flow to the seafloor. During deployment, the bridge plug set prematurely at approximately 466 m below seafloor (mbsf) [*Mikada et al.*, 2002]. The ACORK at ODP Site 808 monitors pressures at six screens. Only two packers are present: one separates the shallowest screen from the seafloor and the other separates the two deepest screens [*Mikada et al.*, 2002]. It is assumed that borehole collapse around screens provides hydraulic isolation for each monitoring interval [*Mikada et al.*, 2003]. Owing to poor drilling conditions at ODP Site 808, the ACORK was emplaced 37 m above its intended position [*Mikada et al.*, 2002]. A bridge plug could not be installed, so the open casing likely accommodates fluid flow between screen 1 and the seafloor [*Mikada et al.*, 2002].

3.2. Lithology and Hydraulic Diffusivity

[15] Four of the five screens at ODP Site 1173 lie in the Lower Shikoku Basin facies (Figure 6), which is composed of moderately bioturbated silty claystone to clayey siltstone. Porosity gradually decreases from approximately 55% at screen 5 (359 mbsf) to 40% at screen 2 (569 mbsf). Screen 1 spans volcaniclastics composed of silty claystone that

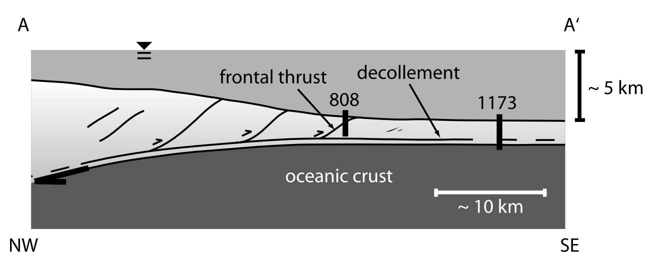

Figure 5. Schematic cross section of Nankai accretionary prism and ACORK locations. The décollement initiates between ODP Sites 808 and 1173. Though the ODP Site 808 borehole penetrates the décollement, the ACORK installation terminates above the décollement.

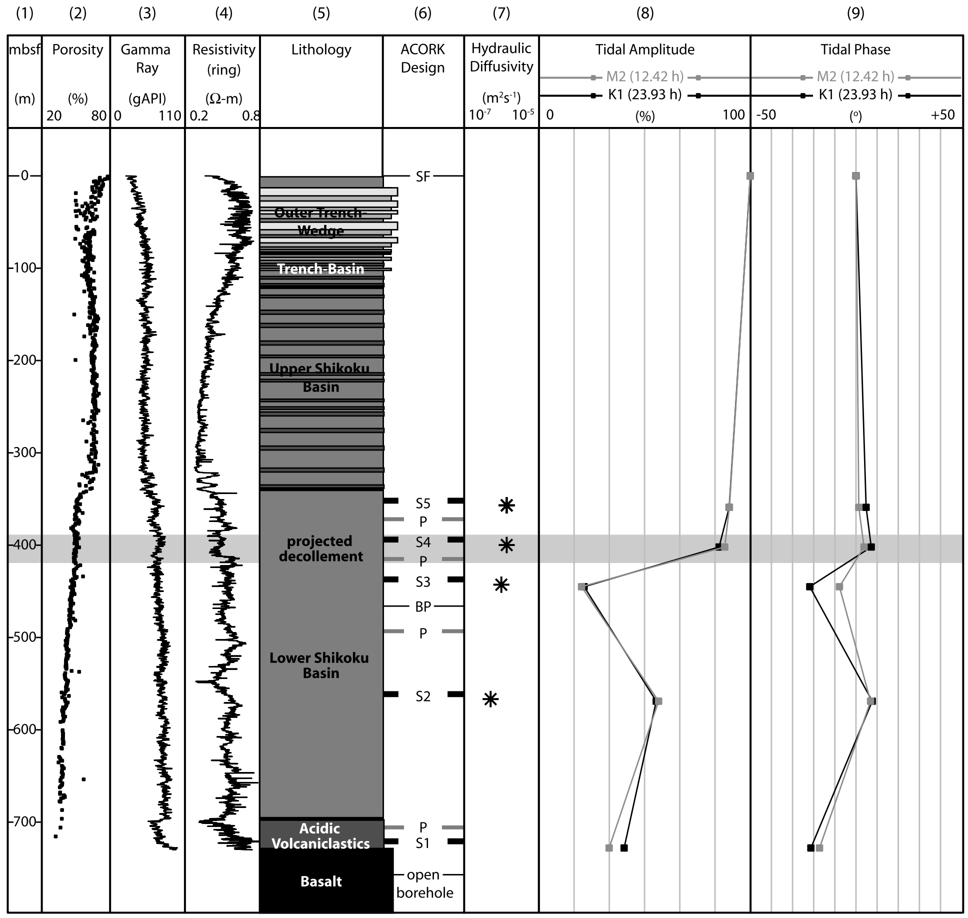

Figure 6. Stratigraphy of ODP Site 1173, ACORK design, and tidal response: (left to right) 1, depth in meters below seafloor; 2, porosity from core samples; 3, logging-while-drilling gamma ray; 4, logging-while-drilling resistivity; 5, stratigraphic units; 6, position of ACORK elements (S, screen; P, packer; and BP, bridge plug); 7, hydraulic diffusivity; 8, tidal amplitude response for K_1 (diurnal) and M_2 (semidiurnal) frequencies; and 9, phase response (Table 3). Porosity, gamma ray, and resistivity data were collected during ODP Legs 190 and 196. Analysis of tidal pressure responses is based on an 80-day window that begins on 12 October 2003.

overlay the oceanic basement (Figure 6) [*Moore et al.*, 2001]. Because screen 1 is close to or in contact with the high-permeability basement, vertical fluid flow from the basement may be significant.

[16] At ODP Site 808, screen 6 lies just above the frontal thrust in the Outer Marginal Trench-Wedge facies, and screen 5 lies below the frontal thrust in the Outer Marginal Trench-Wedge facies of the footwall (Figure 7). The composition of these intervals is bioturbated silty clay and silt turbidites. A thin silt to coarse sand layer occurs at screen 6 (370 mbsf) [*Taira et al.*, 1991]. At screen 5, current-ripple laminated siltstone interbeds are present. Screen 4 lies within the Upper Shikoku Basin facies and spans silty claystone to clayey siltstone with tuff beds. Screens 1 through 3 lie in moderately bioturbated silty claystone to clayey siltstone of the Lower Shikoku Basin facies. Screen 1 is located approximately 10 m above the décollement.

[17] We calculated hydraulic diffusivity at each screen based on estimates of permeability, temperature-dependent fluid viscosity, and formation compressibility (Appendix B and Table 2). At both ACORKs, sand and silt turbidites are less common and porosity generally decreases at greater depths. As a result, permeability decreases with depth by almost 1 order of magnitude at ODP Site 1173 and 4 orders of magnitude at ODP Site 808 (Table 2). Formation compressibility (m_v) varies little with depth, and we assume it equals 10^{-8} Pa^{-1} [*Bourlange et al.*, 2004; D. Saffer et al., unpublished data, 2007].

[18] Because formation compressibility varies little, permeability most strongly influences hydraulic diffusivity at the ACORK screens (Figures 6 and 7). At ODP Site 1173, where four of five screens lie in the Lower Shikoku Basin facies, hydraulic diffusivities decrease slightly from the shallowest to deepest screen (Figure 6). At ODP Site 808, where two screens lie in the Outer Marginal Trench-Wedge facies, hydraulic diffusivities decrease by 4 orders of magnitude (Figure 7).

[19] The small variation in formation compressibility also implies little variation in loading efficiency (γ), which describes the pore pressure response to undrained uniaxial loading. The loading efficiency represents the fraction of an applied load supported by the pore fluid. The loading

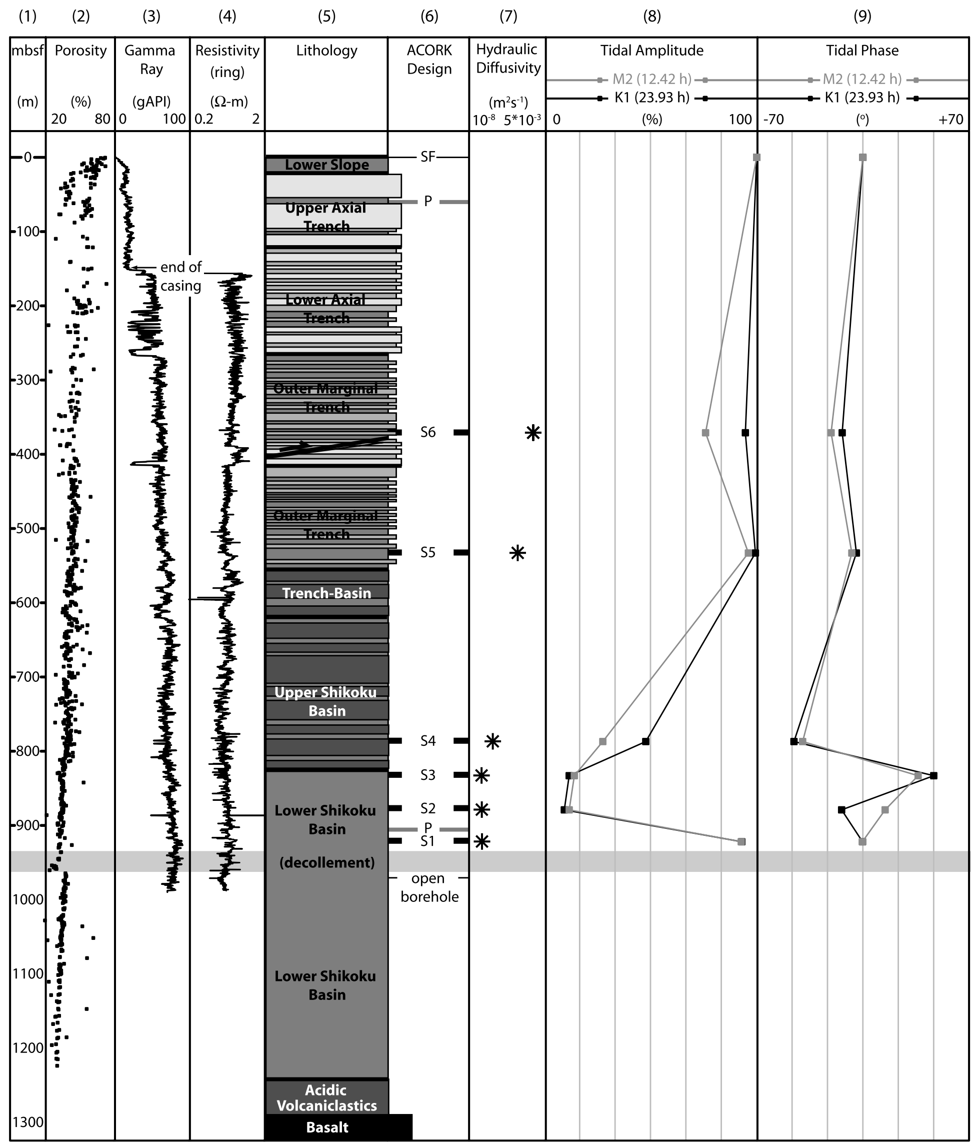

Figure 7. Stratigraphy of ODP Site 808, ACORK design, and tidal response: (left to right) 1, depth in meters below seafloor; 2, porosity from core samples; 3, logging-while-drilling gamma ray; 4, logging-while-drilling resistivity; 5, stratigraphic units; 6, position of ACORK elements (S, screen; and P, packer); 7, hydraulic diffusivity; 8, tidal amplitude response for K_1 (diurnal) and M_2 (semidiurnal) frequencies; and 9, phase response (Table 3). Porosity, gamma ray, and resistivity data were collected during ODP Legs 131 and 196. Analysis of tidal pressure responses is based on an 80-day window that begins on 12 October 2003.

efficiency depends on formation compressibility, porosity, and water compressibility [*van der Kamp and Gale*, 1983; *Wang and Davis*, 1996]:

$$\gamma = \frac{m_v'}{m_v' + n\beta_w}, \tag{9a}$$

where

$$m_v' = \frac{1+\upsilon}{3(1-\upsilon)} m_v. \tag{9b}$$

υ is Poisson's ratio. The sediment at ODP Sites 808 and 1173 has a formation compressibility of 10^{-8} Pa^{-1} [*Bourlange et al.*, 2004; D. Saffer et al., unpublished data, 2007], which is 2 orders of magnitude greater than that of water. For the ACORK monitoring intervals, where porosities range from 0.30 to 0.55, we calculate loading efficiencies between 0.95 and 0.99. This large loading efficiency implies that in situ pore pressure changes approximate changes in the undrained applied load.

3.3. Tidal Response Analysis

[20] We examined two 80-day windows of data: one at ODP Site 1173 (Figure 9) and the other at ODP Site 808 (Figure 10). An 80-day window allows resolution of S_2 (12.00 hours), M_2 (12.42 hours), K_1 (23.93 hours), and O_1 (25.82 hours) frequencies (Figure 11). We calculated the

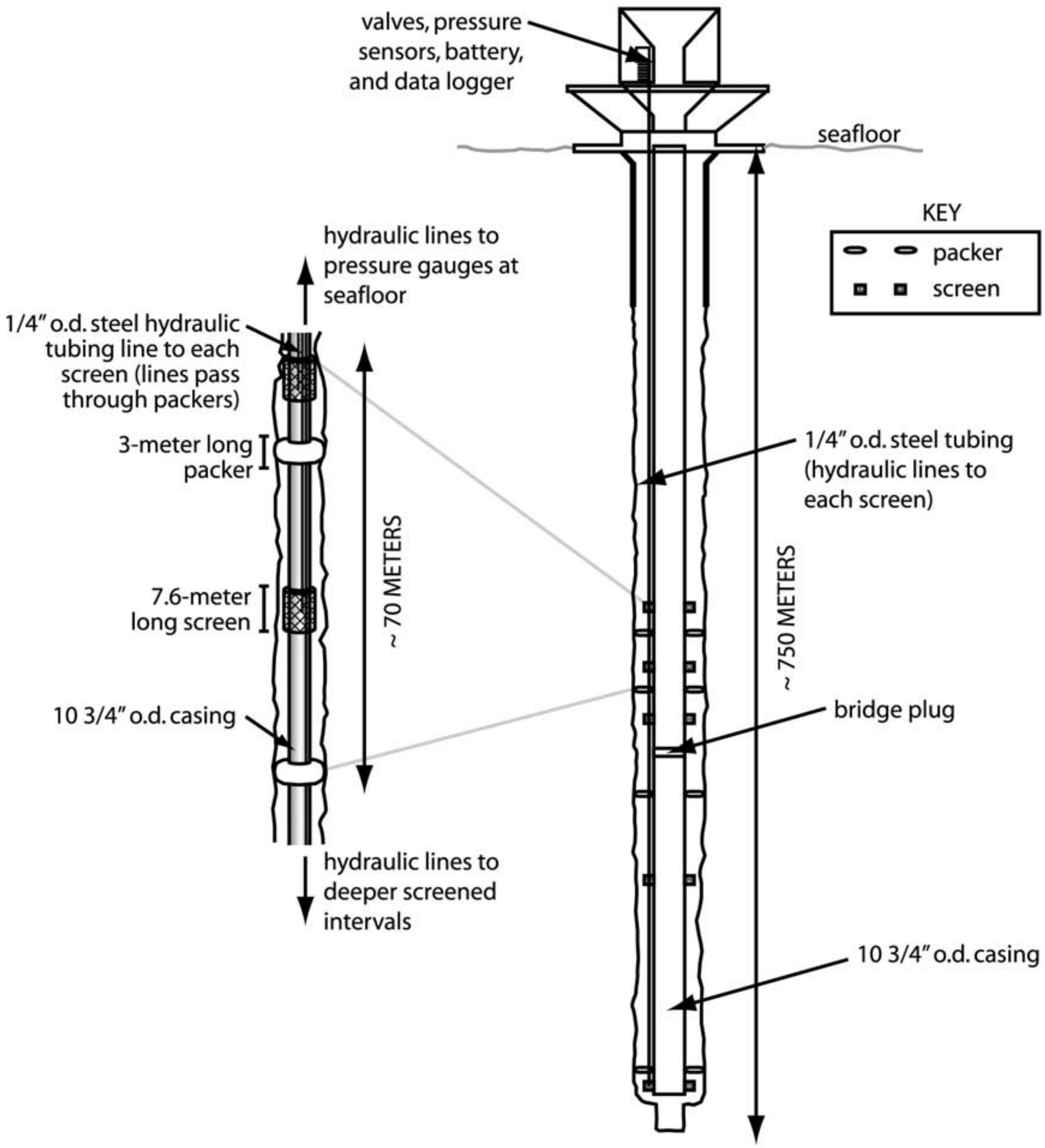

Figure 8. ACORK design at ODP Site 1173. (left) Detailed view of packers and screens. Horizontal exaggeration is approximately 20:1 (screen height is actually 25 times the screen radius). (right) Hydraulic tubing connects screens with pressure sensors at the seafloor. The bridge plug at ODP Site 1173 set prematurely during installation at ~466 m below seafloor (mbsf).

Table 2. Permeability, Viscosity, and Compressibility Estimates Used to Calculate Hydraulic Diffusivity at ODP Sites 1173 and 808[a]

Screen	Depth, mbsf	T, °C	μ, Pa s	k, m^2	m_v, Pa^{-1}	c, m^2 s^{-1}	ω_D (12 hours)	ω_D (24 hours)
1173 S5	359	65	3.9×10^{-4}	8.5×10^{-18}	1.5×10^{-8}	1.4×10^{-6}	2.4	1.2
1173 S4	402	70	3.7×10^{-4}	7.6×10^{-18}	1.5×10^{-8}	1.4×10^{-6}	2.6	1.3
1173 S3	445	78	3.3×10^{-4}	5.1×10^{-18}	1.5×10^{-8}	1.0×10^{-6}	3.5	1.7
1173 S2	569	92	2.9×10^{-4}	2.2×10^{-18}	1.5×10^{-8}	5.1×10^{-7}	6.9	3.5
808 S6	371	41	5.9×10^{-4}	5.0×10^{-15}	1.2×10^{-8}	7.0×10^{-4}	5.0×10^{-3}	2.5×10^{-3}
808 S5	533	54	4.6×10^{-4}	2.6×10^{-16}	1.2×10^{-8}	4.7×10^{-5}	7.6×10^{-2}	3.8×10^{-2}
808 S4	787	72	3.6×10^{-4}	2.4×10^{-18}	1.1×10^{-8}	6.1×10^{-7}	5.8	2.9
808 S3	833	76	3.4×10^{-4}	4.4×10^{-19}	1.5×10^{-8}	8.6×10^{-8}	41	21
808 S2	879	80	3.3×10^{-4}	4.4×10^{-19}	1.5×10^{-8}	9.0×10^{-8}	39	20
808 S1	922	83	3.1×10^{-4}	4.4×10^{-19}	1.5×10^{-8}	9.3×10^{-8}	38	19

[a]See Appendix B; mbsf is meters below seafloor. To calculate ω_D for semidiurnal and diurnal frequencies, we used the ACORK screen radius of 0.156 m.

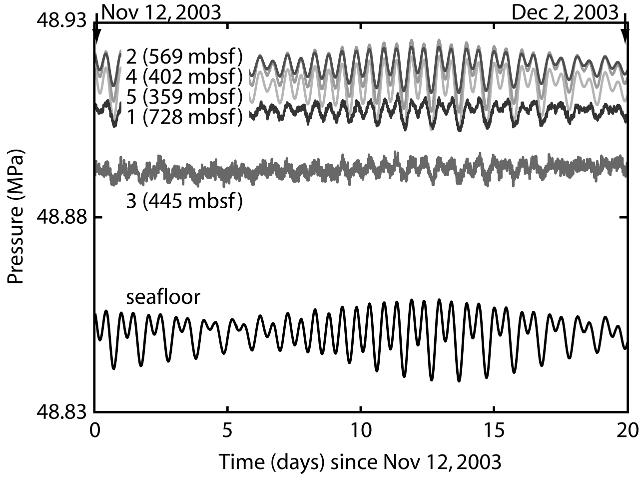

Figure 9. Typical pressure record at ODP Site 1173. Pressure is slightly elevated above hydrostatic (<0.1 MPa) at every screen. Screens 1, 2, and 3 have visibly diminished amplitudes.

amplitude attenuations and phases of semidiurnal and diurnal frequencies at each screen relative to the seafloor using discrete fast Fourier transforms. We report wrapped phase shifts: we match the closest peaks between the screen and seafloor signals. A negative phase shift implies that the screen tidal signal lags the seafloor signal by less than 180° (plus or minus any integer multiple of 360°).

[21] We also examined long-term changes in the average recorded pressures and tidal signals over 3 years of data (2001–2004) at ODP Sites 1173 (Figure 12) and 808 (Figure 13). To track changes in the pressure records, we divided the data into approximately sixty 30-day windows. Consecutive windows overlap by fifteen days. A 30-day window allows resolution of the S_2 and M_2 tidal components. We only plot phase and amplitude of the M_2 tidal component since it has the highest signal-to-noise ratio (Figure 11).

3.3.1. ODP Site 1173 Tidal Responses

[22] Tidal signals at ODP Site 1173 generally decrease in amplitude with depth (Figure 6 and Table 3). At screens 4 and 5, amplitudes approach 90% of tidal loading amplitudes, as predicted in the compressible Lower Shikoku Basin facies. In contrast, screens 1, 2, and 3 have small amplitudes (35%, 55%, and 20% of loading amplitudes, respectively). Screens 1 and 3 also have large negative phase shifts (−30°), while the other screens have small positive phases (∼ +5°).

[23] The M_2 (12.42 hours) amplitudes and phases vary with time (Figure 12). During ACORK installation, valves for screens 3, 4, and 5 rotated open. In August 2002 when the first pressure data were recovered, the open pump valves were discovered and closed [*Mikada et al.*, 2003]. Pressure at screen 1 inexplicably fell, though the valve for this screen was not disturbed. The elevated pressure, small amplitudes, and large phase lags at screen 1 indicate that either the bridge plug or borehole collapse isolates the screen from the seafloor. The slow pressure recovery after valve closure at screen 3 may suggest the permeability is especially low. The small amplitudes and large phase lags also imply a reduced permeability at screen 3.

3.3.2. ODP Site 808 Tidal Responses

[24] Tidal signals at ODP Site 808 also decrease in amplitude with depth. Amplitudes at screens 2 and 3 (in low-permeability hemipelagic mudstone) are less than 15% of tidal loading amplitudes. However, amplitudes at screens 5 and 6 (in silty hemipelagic turbidites) approach 90% of tidal loading amplitudes, as predicted for compressible sediment (Figure 7). Phase lags increase with depth from screen 6 (−15°) to screen 4 (−40°). However, screens 2 and 3 have large phase leads (Figure 7 and Table 3).

[25] The M_2 tidal signals at ODP Site 808 also vary through time. The pump valve for screen 3 was the only valve found closed at ODP Site 808 in August 2002 [*Mikada et al.*, 2003]. As a result, all other screens recorded hydrostatic pressures, zero phase shifts, and no amplitude attenuation prior to valve closure (Figure 13). After valve closure, mean pressures at screens 1 and 2 (Lower Shikoku Basin facies) rose (Figure 13a). Screen 4 (Upper Shikoku Basin facies) and screens 5 and 6 (Outer Marginal Trench-Wedge facies) all maintained hydrostatic pressures from 2002 to 2004.

3.4. Formation-Instrument Compliance Ratio (β_D)

[26] One interpretation of small amplitudes and large phase shifts in measured tidal pressure responses is that the instrument is sufficiently compliant, given the hydraulic diffusivity of the formation, to impact the fidelity of the measurements. To evaluate this interpretation, we estimated the formation-instrument compliance ratio for the ACORKs through three approaches.

3.4.1. Formation-Instrument Compliance Ratio (β_D) From Tidal Response

[27] We used observed amplitude attenuations and phases to estimate β_D. We represent K_1 (diurnal) and M_2 (semidiurnal) tidal amplitudes and phases at each screen as horizontal bars (Figure 3). Solid bars indicate K_1 (diurnal) frequencies, and dashed bars indicate M_2 (semidiurnal) frequencies. The vertical position of each bar corresponds

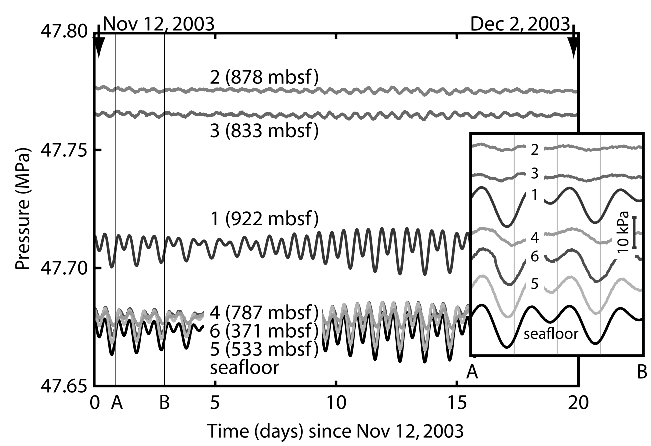

Figure 10. Typical pressure record at ODP Site 808. Pressure is slightly elevated above hydrostatic (<0.2 MPa) at screens 2 and 3. Inset shows mean-removed pressures over the 2-day window A–B. Screens 2, 3, and 4 have visibly diminished amplitudes and large phase shifts.

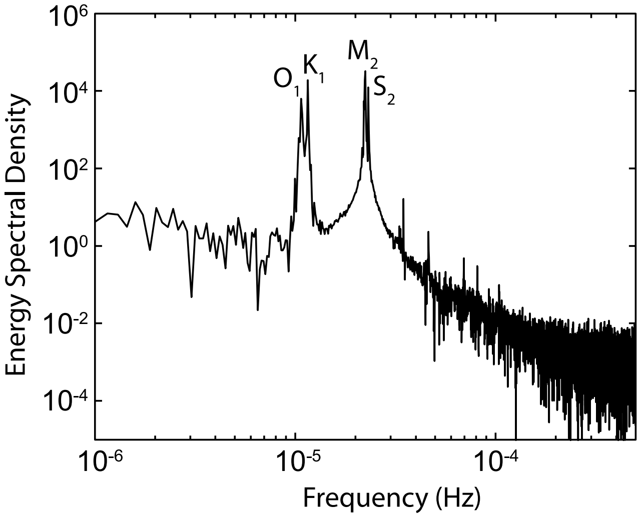

Figure 11. Spectral energy distribution for the seafloor signal at ODP Site 808. The frequencies with the greatest energy are semidiurnal (S_2 and M_2) and diurnal (O_1 and K_1) tidal frequencies.

to the amplitude (Figure 3a) or phase (Figure 3b) measured at that screen (Table 3). Each bar spans a 1-order-of-magnitude range in ω_D, which corresponds to a 1-order-of-magnitude uncertainty in our permeability estimates (Table 2). We used vertical permeability estimates to calculate hydraulic diffusivity and ω_D (Table 2). Horizontal permeability may be up to ten times greater [*Yang and Aplin*, 2007]. We excluded ODP Site 808 screen 1 and ODP Site 1173 screen 1 from our analysis because of the potential for drainage to the seafloor and basement, respectively.

[28] All but one of the screens lie along an amplitude response curve with characteristic β_D between 0.1 and 1 (Figure 3a). Three of the nine analyzed screens also lie on a phase shift curve with characteristic β_D between 0.1 and 1 (Figure 3b). We did not plot screens with positive phases on Figure 3b, as our model does not predict positive phases. We used equation (2b) to estimate β^*V (wellbore storage) from our estimate of β_D, the ACORK screen dimensions (a and h) (Appendix B), and formation compressibility (m_v) (Table 2). Because a, h, and m_v are similar for all screens, so is the wellbore storage. If $\beta_D = 0.5$, β^*V is 2×10^{-8} m^3 Pa^{-1} at both ACORK sites (equation (2b)).

3.4.2. Formation-Instrument Compliance Ratio (β_D) From ACORK Design

[29] To determine whether this wellbore storage estimate is realistic, we calculated the wellbore storage (β^*V) from the known geometry and material properties of the ACORKs (equation (2b), Table 4, and Appendix C). We assumed the only source of instrument compressibility to be the water-filled steel hydraulic tubing and steel inner casing. We calculated β^*V to be 8×10^{-11} m^3 Pa^{-1}. Given a formation compressibility (m_v) of 1.5×10^{-8} Pa^{-1}, β_D is thus 200 (Appendix C). We indicate the predicted semidiurnal tidal pressure response for ODP Site 808 screen 2 in Figure 3 (open stars).

3.4.3. Formation-Instrument Compliance Ratio (β_D) From Well Test Analysis

[30] On 6 August 2002 (4 d after valve closure in Figure 13), a remotely operated vehicle opened and promptly closed the pump valve for ODP Site 808 screen 2 [*Mikada et al.*, 2003] (Figure 14a). The pressure at screen

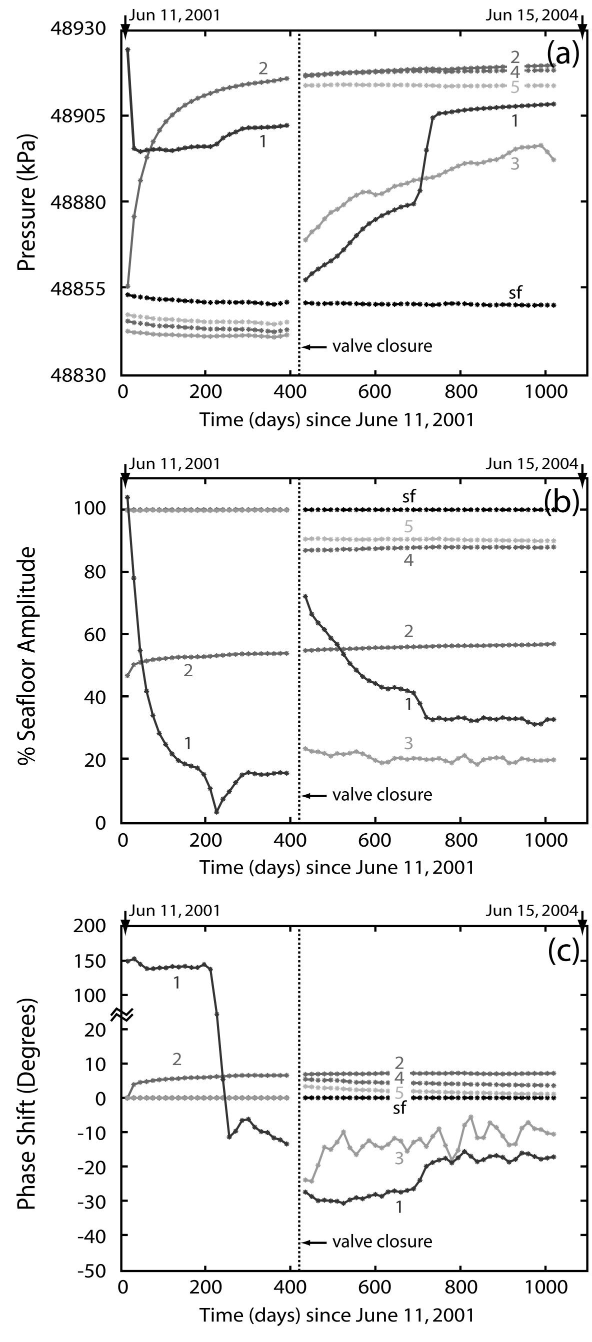

Figure 12. (a) Mean pressure versus time since installation at ODP Site 1173. (b) Amplitude response versus time for the M_2 (semidiurnal) tidal signal. (c) Phase shift versus time for the M_2 (semidiurnal) tidal signal. Open pump valves for screens 3, 4, and 5 were discovered and closed at approximately 400 days. Elevated fluid pressures, small amplitudes, and large phase shifts at screen 1 indicate that the bridge plug seals the inner casing and isolates screen 1 from the seafloor.

Table 3. Measured Tidal Pressure Responses at ODP Sites 1173 and 808, Based on an 80-Day Window That Begins on 12 October 2003[a]

	Amplitude, %				Phase Shift, deg			
Screen	O_1 (25.82 hours)	K_1 (23.93 hours)	M_2 (12.42 hours)	S_2 (12.00 hours)	O_1 (25.82 hours)	K_1 (23.93 hours)	M_2 (12.42 hours)	S_2 (12.00 hours)
1173 SF	100.00	100.00	100.00	100.00	0.00	0.00	0.00	0.00
1173 S5	88.99	90.04	90.13	90.35	5.1713	4.7960	1.3266	1.1750
1173 S4	83.96	85.26	87.91	88.74	7.2433	7.2184	3.8061	3.8016
1173 S3	25.09	21.42	20.19	20.44	−22.467	−21.857	−7.814	−8.189
1173 S2	55.72	55.53	56.65	57.15	4.1406	7.6981	6.9092	10.409
1173 S1	42.28	40.34	33.25	33.66	−17.888	−21.330	−17.244	−17.667
808 SF	100.00	100.00	100.00	100.00	0.00	0.00	0.00	0.00
808 S6	101.18	94.68	75.94	76.53	−14.146	−13.626	−20.941	−20.290
808 S5	99.73	99.41	96.10	95.55	−4.286	−4.269	−7.279	−7.474
808 S4	51.20	47.78	27.56	27.27	−46.803	−45.415	−39.695	−38.856
808 S3	10.42	11.72	14.16	14.52	54.008	46.726	36.429	35.844
808 S2	8.21	9.43	11.74	12.29	−25.551	−14.000	14.674	15.273
808 S1	92.96	92.99	92.73	92.65	−0.3131	−0.2129	−0.3522	−0.3247

[a]Amplitudes are indicated as percentages of seafloor amplitudes for four tidal frequencies. The phase shifts (degrees) are relative to phases at the seafloor.

2 immediately dropped to hydrostatic and then asymptotically approached a new pressure approximately 100 kPa above hydrostatic. In an ideal slug test, instrument pressure is instantaneously offset from formation pressure and then allowed to recover. Formation pressure should be uniform near the screen prior to the slug test [*Neuzil*, 1982]. Unfortunately, at ODP Site 808 screen 2, open flow from 2001 to 2002 had likely reduced formation pressures around the screen (Figure 14a).

[31] Nonetheless, we interpret this pressure response as a traditional slug test, since it is the closest approximation to a well test conducted at either ACORK. The data match a type curve with characteristic β_D of 0.01 (Figure 14b). This β_D implies a wellbore storage ($\beta^* V$) of 2×10^{-6} m^3 Pa^{-1}, given the screen geometry and formation compressibility of 1.5×10^{-8} Pa^{-1}. The match between the data and type curve also establishes ca^{-2} as 0.0026 s^{-1} (Figure 14b). Given an ACORK screen radius (a) of 0.156 m, c is thus 6.3×10^{-5} m^2 s^{-1}. Using our ca^{-2} value, we determined ω_D for a semidiurnal tidal frequency to be 0.056 (equation (6b)). We indicate the tidal pressure response for the slug test-derived β_D and ω_D estimates in Figure 3 (solid stars).

4. Discussion

[32] At ODP Sites 808 and 1173, tidal amplitudes and hydraulic diffusivities generally decrease with depth (Figures 6 and 7). Most of the measured amplitudes in the Lower Shikoku facies are much smaller than amplitudes predicted for the formation (~95% of seafloor amplitudes). Phase shifts also become large (nonzero) as diffusivity decreases. We interpret that small amplitudes and large phase shifts result from hydraulic impedance at the screens. A formation-instrument compliance ratio (β_D) of 0.5, and consequently a wellbore storage ($\beta^* V$) of 2×10^{-8} m^3 Pa^{-1}, will reconcile most of the tidal measurements, given our hydraulic diffusivity estimates (Table 2). This β_D value implies a dimensionless critical frequency of 0.07 (Figure 3a). In the Lower Shikoku Basin facies ($c \sim 10^{-7}$ m^2 s^{-1}), the dimensionless critical frequency equates to 5×10^{-8} Hz, or a period of 250 days. Measured pressure signals with shorter periods will theoretically have attenuated amplitudes and phase shifts, given our wellbore storage estimate. For example, at the Nyquist frequency ($\sim 10^{-3}$ Hz), our model predicts an amplitude response near 1% and a phase lag near $-45°$ in the Lower Shikoku Basin facies.

[33] In spite of their low critical frequencies, the ACORKs will record a rapid pressure change in response to a nearly instantaneous formation pressure change. The pressure response follows the step load solution (Figure 2). For $\beta_D \sim 0.5$, measured pressures will equilibrate to within 90% of the formation pressure change (ε = 0.1) at a dimensionless time (t_D) of approximately 12 (Figure 2, $\beta_D t_D$ = 6). At ODP Site 1173, this dimensionless time is equivalent to three days at screen 5, where diffusivity is greatest, and seven days at screen 1, where diffusivity is least (equation (1d) and Table 2). This calculation agrees well with rapid pressure changes observed at ODP Site 1173 following VLF earthquake activity in 2003 [*Davis et al.*, 2006, Figure 4]. Pressures declined at ODP Site 1173 screens 2, 4, and 5 over approximately 5 days, while pressure at screen 1 increased over approximately 6 d.

[34] Our wellbore storage estimate from tidal responses lies between two other independent estimates. The slug test (Figure 14b) implies a very compressible instrument with $\beta^* V \sim 10^{-6}$ m^3 Pa^{-1} and $\beta_D \sim 10^{-2}$. Most likely, this apparent compressibility results from significant pressure drawdown around the wellbore prior to the test. The cone of depression causes a slower pressure recovery than predicted and thus an apparently high wellbore storage value.

Table 4. ACORK Engineering Specifications for Calculation of β_D at ODP Site 808 Screen 2[a]

Variable	Definition	Dimension
m_v	formation compressibility	1.5×10^{-8} Pa^{-1}
r_{t_i}	tube inner radius	0.0023 m
r_{t_o}	tube outer radius	0.0032 m
β_{steel}	steel compressibility	5.0×10^{-12} Pa^{-1}
β_w	fluid compressibility	4.5×10^{-10} Pa^{-1}
r_{s_i}	screen inner radius	0.136 m
r_{s_o}	screen outer radius	0.156 m
h	screen height	7.6 m
r_{c_i}	casing inner radius	0.126 m
r_{c_o}	casing outer radius	0.136 m
L_t	tubing length	878 m

[a]See Appendix C.

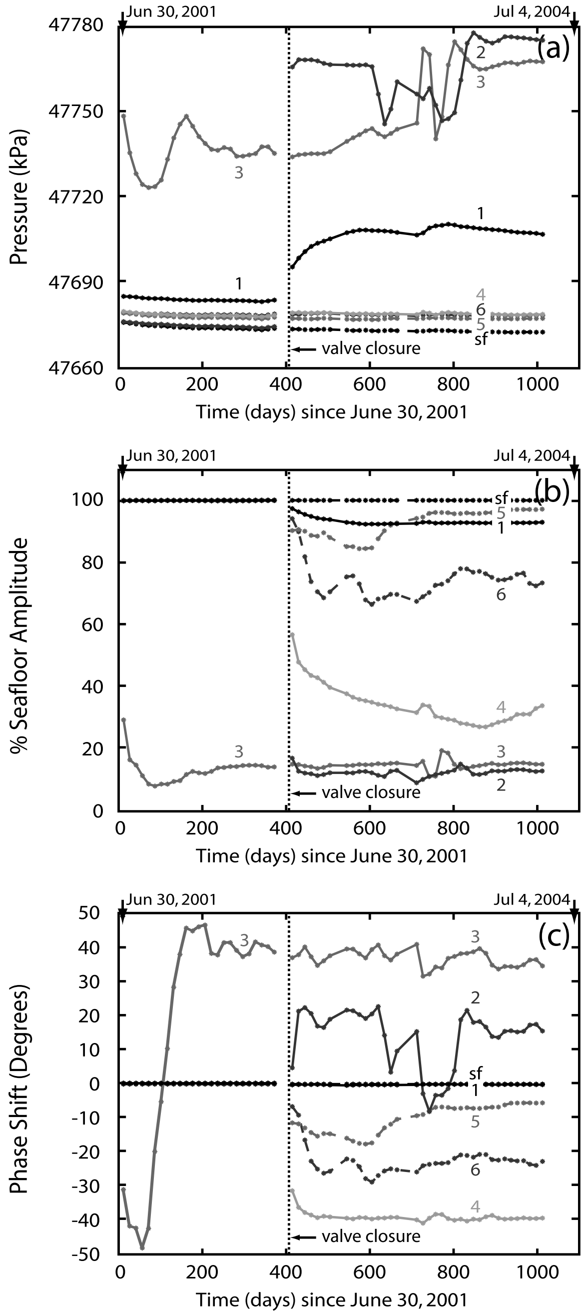

Figure 13. (a) Mean pressure versus time since installation at ODP Site 808. (b) Amplitude response versus time for the M_2 (semidiurnal) tidal signal. (c) Phase versus time for the M_2 (semidiurnal) tidal signal. Open pump valves for screens 1, 2, 4, 5, and 6 were discovered and closed at approximately 400 days. Average pressures varied at screens 2 and 3 (Lower Shikoku Basin facies) over the 3-year record. Major transient pulses, interpreted as responses to deformation events [*Davis et al.*, 2006], occurred at screens 2, 3, and 4 in the Lower Shikoku Basin and Upper Shikoku Basin facies during this period ($\sim$725 days).

[35] In contrast, our calculation of wellbore storage from the ACORK design (Appendix C) implies a very stiff instrument with $\beta^* V \sim 10^{-10}$ m^3 Pa^{-1} and $\beta_D \sim 10^2$. This calculation likely underestimates the system compressibility. Closed monitoring systems often have unexpectedly large system compressibilities due to instrument parts and connections [*Neuzil et al.*, 1981; *Neuzil*, 1982]. Potential sources of ACORK compliance that we ignored in our calculation include the screens and packers, as well as numerous connections in the hydraulic lines that transmit screen pressures to the gauges (Figure 8). Leaky hydraulic connections are common in experimental systems [*Neuzil et al.*, 1981; *Neuzil*, 1982]. Free gas in the tubing or screens would also increase β^*, although the effect would be small at confining pressures near 50 MPa [*Wang et al.*, 1998].

[36] Alternatively, if hydraulic diffusivities are 1000 times less than our estimates (Table 2), tidal analysis will predict the same β_D as our calculation from ACORK design because tidal responses will plot further to the right (at higher ω_D values) in Figure 3. In mudstones, drilling can shear borehole walls to create a low-permeability zone (Figure 1, light shading) [*d'Astous et al.*, 1989; *Fisher et al.*, 1996; *Fisher and Zwart*, 1997]. The damaged zone permeability determines ω_D if the damaged zone is thicker than the penetration distance of a tidal pressure signal. The diffusion length (L) defines the penetration distance:

$$L = \sqrt{ct}. \tag{10}$$

For a 12-hour period in the undamaged Lower Shikoku Basin facies ($c \sim 10^{-7}$ m^2 s^{-1}), L is 6 cm. For a 1000-fold reduction in permeability within the damaged zone, L is 2 mm. Therefore a thin zone of severe damage in combination with a stiff instrument can explain the observed amplitudes and phases.

[37] We assumed horizontal flow into a cylindrical cavity from a homogeneous medium and did not consider the effect of flow contributions from above and below the screened interval. To evaluate the impact of vertical flow to the screen, we numerically modeled the same problem in spherical coordinates. We represented the cylindrical screen as a sphere with an equivalent surface area. The results approximated those of the cylindrical coordinate system, even for screens with a height-to-radius ratio as large as 25 (Figure 3, solid and open circles).

[38] Our model is most appropriate for instruments that monitor pressures far from a drainage boundary such as the seafloor or high-permeability basement. Close to a drainage boundary (within the diffusive wavelength of a tidal signal), vertical fluid exchange across the drainage boundary influences the in situ tidal pressure response [*van der Kamp and Gale*, 1983; *Rojstaczer and Riley*, 1990; *Wang and Davis*, 1996]. The diffusive wavelength for the Lower Shikoku Basin facies is 6 cm. Even for the greatest hydraulic diffusivity we estimate (7×10^{-4} m^2 s^{-1}) the diffusive wavelength is only 5 m. All screens we included in our analysis are over 100 m from the seafloor or basement. Thus vertical drainage is negligible.

[39] Our model cannot predict phase lags greater than $-90°$ or phase leads of any form, yet we observe small phase leads at ODP Site 1173 screens 2, 4, and 5 and larger leads at ODP Site 808 screens 2 and 3. One-dimensional tidal loading models predict attenuated amplitudes and phase leads near a contrast in compressibility where the framework stiffness or pore fluid compressibility increases [*van der Kamp and Gale*, 1983; *Wang and Davis*, 1996].

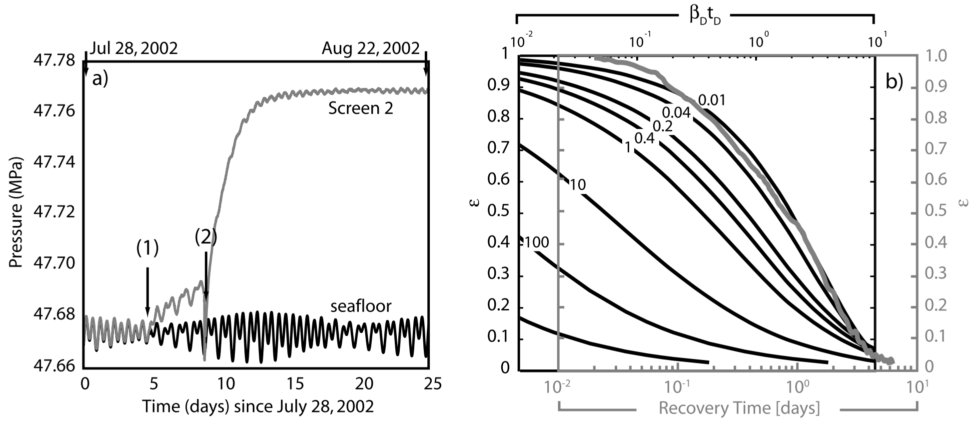

Figure 14. (a) Pressure record at the seafloor and ODP Site 808 screen 2 during inadvertent slug test. The valve for screen 2 had been open prior to 2 August 2002 (labeled 1). The valve was closed (labeled 1), and pressure began to recover. Before pressure had fully equilibrated, the valve was quickly opened and closed again (labeled 2). Measured pressures recovered over days. (b) Shaded plot showing equilibration, ε (equation (5)), at ODP Site 808 screen 2 versus time, beginning after the second valve closure (labeled 2). The solid curves are dimensionless pressure response curves (Figure 2). The data match a type curve with characteristic β_D of 0.01. The offset between the t axis of the data plot and the $\beta_D t_D$ axis of the type curve plot establishes ca^{-2} as 0.0026 s^{-1} (equation (1d)).

However, these models generally do not predict positive phase shifts greater than 20° or amplitudes as small as 10% in compressible sediment under high (>20 MPa) confining pressures (even near accumulations of free gas) [*Wang et al.*, 1998]. Thus free gas cannot explain the recorded phase leads and amplitude attenuations in the ACORK data.

[40] *Davis and Becker* [2007] recently suggested an alternate explanation for both tidal signals and transient pressure pulses at ODP Site 808. They proposed that tidal or tectonic forcing pumps warm formation fluid into and out the bottom of the unsealed casing at ODP Site 808. The displacement of warm fluid inside the casing alternately warms the surrounding tubing and screens to produce a measurable pressure perturbation. This model is intriguing because it presents an alternate mechanism for amplitude and phase modulation of measured pressure signals and because it also relies on low hydraulic diffusivity at monitoring intervals. Moreover, the thermal compliance model can generate phase leads, unlike our mechanical compliance model. It may also explain the presence of coherent, high-frequency, low-amplitude signals at some of the ACORK screens (Figure 10, screens 2, 3, 4, and 6).

[41] Our analysis of the *Davis and Becker* [2007] model suggests that phase is particularly sensitive to thermal forcing, and amplitude is less sensitive. This sensitivity might explain why amplitude responses cluster more closely along a characteristic β_D curve than phase shifts (Figure 3). Ultimately, thermal forcing cannot explain all amplitudes and phase shifts in the ACORK data [*Sawyer*, 2007]. A critical observation is that ODP Site 1173 screens 2 and 3 lie in the low-diffusivity Lower Shikoku Basin facies and have amplitude responses as small as 55% and 20%. Yet the bridge plug at ODP Site 1173 presumably seals the casing and prevents thermal pressure perturbations (Figure 8).

[42] Direct experiments would clarify the contributions of thermal and mechanical compliance to the ACORK pressure response. Through slug tests, we could measure hydraulic diffusivity and wellbore storage in situ. Proper slug test procedure includes measuring the fluid volume added or removed during the test [*Neuzil*, 1982]. Late time analysis of slug test results determines two of three variables, given an assumption of the third: wellbore storage (β^*V), hydraulic diffusivity (c), and a measure of formation damage (S_w) [*Sageev*, 1986]. Additionally, we have hoped for several years to install a bridge plug at ODP Site 808. Sealing the annulus at ODP Site 808 would eliminate fluid flow in the casing and associated thermal perturbations.

[43] We have presented a systematic approach to understand pore pressure measurements in low-diffusivity sediment. We have applied this approach to analyze data from the Nankai ACORKs. Ultimately, our analysis does not reconcile all the data but does suggest that where hydraulic diffusivities at monitoring intervals are low, mechanical compliance impacts the fidelity of measured pressures signals with high frequencies. Results from new slug tests may influence the design and experimental application of present and future marine pressure monitoring systems. Our analyses suggest that in hemipelagic mud, the ACORK wellbore storage is too large to permit accurate measurement of in situ pressures at tidal frequencies. Future actions to improve pressure measurements may include (1) designing well tests into CORK experimental plans to support interpretation of pressure data, (2) designing stiffer instrument systems with smaller volumes, or (3) increasing permeabilities near screens in future installations with sand packs, hydraulic fractures, or conventional well development.

5. Conclusions

[44] In the Nankai ACORKs (offshore Japan), measured pressures have amplitudes as low as 10% of the amplitude of the tidal load and phase shifts of more than 25°. These measurements occur in thick, homogeneous, compressible,

low-permeability sediment, where in situ pressure signals should approximate the tidal load. To determine the fidelity of these pressure measurements, we used a quantitative model for the response of a closed monitoring instrument to formation pressure changes. The measured pressure response to a change in formation pressure depends on the formation-instrument compliance ratio (β_D), hydraulic diffusivity, and the frequency of the pressure signal. At the Nankai ACORKs, a wellbore storage of 2×10^{-8} m^3 Pa^{-1} can explain many of the observed tidal responses, given the hydraulic diffusivities of the monitored intervals. A reduced permeability around the borehole of 1000-fold and a wellbore storage of 10^{-11} m^3 Pa^{-1} can also reconcile the data. Our analysis suggests that ACORK screens in the Lower Shikoku Basin facies have a critical frequency on the order of 5×10^{-8} Hz (equivalent to a period of 250 days). Formation pressure signals with greater frequencies will be distorted in the pressure record. We also estimate that the time for the ACORKs to record 90% of an instantaneous pressure change in the Lower Shikoku Basin facies is on the order of 10 days.

[45] We have presented an approach to quantify the impact of mechanical compliance and hydraulic diffusivity on pressure measurements at submarine hydrologic monitoring stations. Our analysis of the Nankai ACORKs illustrates that in low-diffusivity sediment, the fidelity of pressure measurements is sensitive to instrument compressibility when pressure signals contain high frequencies. We recommend conducting slug tests at submarine monitoring instruments installed in low-diffusivity sediment to aid quantification of instrument response.

Appendix A: Parameters for Sinusoidal Loading Equations

[46] The amplitude and phase of a sinusoidal pressure change measured by a closed instrument (equation (8)) are dependent on imaginary parameters E and F:

$$E = 1 - \frac{\omega_D}{\beta_D}[\Psi Ker(\sqrt{\omega_D}) + \Phi Kei(\sqrt{\omega_D})], \tag{A1}$$

$$F = \frac{\omega_D}{\beta_D}[\Phi Ker(\sqrt{\omega_D}) + \Psi Kei(\sqrt{\omega_D})]. \tag{A2}$$

$Ker(x)$ and $Kei(x)$ are Kelvin functions of order 0. Ψ and Φ are given by

$$\Phi = -\frac{\left[Ker_1\left(\sqrt{\omega_D}\right) + Kei_1\left(\sqrt{\omega_D}\right)\right]}{\sqrt{2\omega_D}\left[Ker_1^2\left(\sqrt{\omega_D}\right) + Kei_1^2\left(\sqrt{\omega_D}\right)\right]}, \tag{A3}$$

$$\Psi = -\frac{\left[Ker_1\left(\sqrt{\omega_D}\right) - Kei_1\left(\sqrt{\omega_D}\right)\right]}{\sqrt{2\omega_D}\left[Ker_1^2\left(\sqrt{\omega_D}\right) + Kei_1^2\left(\sqrt{\omega_D}\right)\right]}. \tag{A4}$$

$Ker_1(x)$ and $Kei_1(x)$ are Kelvin functions of order 1.

Appendix B: Hydraulic Diffusivity Calculations

[47] We estimated hydraulic diffusivity at each screen based on permeability, formation compressibility, and temperature-dependent fluid viscosity (equations (1e) and (1f) and Table 2). For screens in the Upper and Lower Shikoku Basin facies, we estimated permeability from laboratory measurements on samples with similar porosities [*Gamage and Screaton*, 2003, 2006]. We also calculated permeability using an empirical permeability-porosity relationship [*Gamage and Screaton*, 2003, 2006]:

$$\log k = -19.82 + 5.39n. \tag{B1}$$

[48] For screens in interbedded silts and muds, we used RAB images [*Mikada et al.*, 2002] and core descriptions [*Taira et al.*, 1991] to estimate total silt bed thickness at each screen. We then calculated weighted average screen permeabilities based on typical marine mudstone and siltstone permeabilities [*Freeze and Cherry*, 1979]. For example, ODP Site 808 screen 5 lies in hemipelagic mud interbedded with four very thin to thin normally graded silt layers [*Taira et al.*, 1991]. We assumed mud and silt permeabilities of 10^{-18} m^2 and 10^{-14} m^2, respectively [*Freeze and Cherry*, 1979]. For a 7.6-m screen interval with four 5-cm-thick silt beds, the permeability is thus 2.6×10^{-16} m^2 (Table 2). For comparison, *Adatia and Maltman* [2004] estimated a similar permeability (9.6×10^{-17} m^2) for an Outer Marginal Trench-Wedge facies core sample at ODP Site 1174.

[49] Formation compressibility (m_v) varies little with depth, according to the few estimates from laboratory tests on core samples. In Outer Marginal Trench-Wedge and Shikoku Basin facies sediment, m_v is typically 10^{-8} Pa^{-1} [*Bourlange et al.*, 2004; D. Saffer et al., unpublished data, 2007]. If we assume the pore fluid is water, which has a compressibility of 4×10^{-10} Pa^{-1}, the storage coefficient approximates the product of specific weight and formation compressibility (equation (1f)).

[50] We calculated fluid viscosity (μ) after *Gartling* [1977]:

$$\mu = 16.68T^{-0.8987}, \tag{B2}$$

where T is temperature in degrees Celsius. We used temperature projections from measurements above 400 mbsf at ODP Sites 808 and 1173 [*Taira et al.*, 1991; *Moore et al.*, 2001].

Appendix C: ACORK Wellbore Storage Calculation

[51] We calculated the ACORK formation-instrument compliance ratio (β_D) from equation (2b). We assumed a formation compressibility (m_v) for the Lower Shikoku Basin facies to be 1.5×10^{-8} Pa^{-1} (Appendix B). We calculated V and β^* from ACORK specifications in Table 4 (equations (C1) and (C2)).

[52] The ACORK screens are cylindrical shells that surround the inner casing: each screen stands 7.6 m high and has a thickness of 2 cm (Figure 8). The ACORK volume, V, is the volume of the screen (first term) and hydraulic tubing (second term):

$$V = \pi\left(r_{s\_o}^2 - r_{s\_i}^2\right)h + \pi r_{t\_i}^2 L_t, \tag{C1}$$

where r_{s_o} is the screen outer radius, r_{s_i} is the screen inner radius, h is the screen height, L_t is the tubing length to the seafloor, and r_{t_i} is the inner tubing radius. At ODP Site 808 screen 2, the tubing length is 878 m. The total volume is 0.15 m^3.

[53] The ACORK system compressibility is the sum of the fluid compressibility (β_w), steel tubing compressibility (second term), and casing compressibility (third term):

$$\beta^* = \beta_w + \beta_{steel}\left(\frac{r_{t\_o}}{r_{t\_o} - r_{t\_i}} + \frac{r_{c\_o}}{r_{c\_o} - r_{c\_i}}\right). \quad \text{(C2)}$$

We did not attempt to estimate additional sources of compressibility such as screens, hydraulic connections, and packers. For β_w, we assumed the compressibility of water (4.5×10^{-10} Pa^{-1}). The tubing compressibility is a function of the compressibility of steel (β_{steel}) and the tubing dimensions, while the inner casing compressibility is a function of the compressibility of steel and casing dimensions. β^* is 5×10^{-10} Pa^{-1}. Substituting V and β^* into equation (2b), we calculated β_D to be $\sim$200.

[54] **Acknowledgments.** Core samples and borehole logging data were provided by the Ocean Drilling Program (ODP). The Japanese Agency for Marine Technology (JAMSTEC) generously provided use of research vessels and submersibles for ACORK data recoveries. We thank Turgay Ertekin for helpful suggestions in well test analysis and Earl Davis and Robert Meldrum for fruitful discussions. We thank Andrew Fisher, Elizabeth Screaton, Tomochika Tokunaga, an anonymous reviewer, and the Associate Editor for their valuable reviews. This research was supported by NSF EAR 0447235, U.S. Science Support Program funds for ODP Leg 196, and the Penn State GeoFluids Consortium.

References

Adatia, R. H., and A. J. Maltman (2004), Data report: Initial permeability determinations on sediments from the Nankai Trough accretionary prism, ODP Sites 1173 and 1174 online, *Proc. Ocean Drill. Program Sci. Results*, *190/196*, 12 pp. (Available at http://www-odp.tamu.edu/publications/190196SR/214/214.htm)

Becker, K., and E. E. Davis (2005), A review of CORK designs and operations during the Ocean Drilling Program, *Proc. Integr. Ocean Drill.*, *301*, doi:10.2204/iodp.proc.301.104.2005.

Becker, K., A. T. Fisher, and E. E. Davis (1997), The CORK experiment in Hole 949C: Long-term observations of pressure and temperature in the Barbados accretionary prism, *Proc. Ocean Drill. Program Sci. Results*, *156*, 247–252.

Bourlange, S., L. Jouniaux, and P. Henry (2004), Data report: Permeability, compressibility, and friction coefficient measurements under confining pressure and strain, Leg 190, Nankai Trough online, *Proc. Ocean Drill. Program Sci. Results*, *190/196*, 16 pp. (Available at http://www-odp.tamu.edu/publications/190196SR/VOLUME/CHAPTERS/215.PDF)

Bredehoeft, J. D. (1967), Response of well-aquifer systems to Earth tides, *J. Geophys. Res.*, *72*, 3075–3087.

Bredehoeft, J. D., and S. S. Papadopulos (1980), A method for determining the hydraulic properties of tight formations, *Water Resour. Res.*, *16*, 233–238.

Cooper, H. H., Jr., J. D. Bredehoeft, I. S. Papadopulos, and R. R. Bennett (1965), The response of well-aquifer systems to seismic waves, *J. Geophys. Res.*, *70*, 3915–3926.

Cooper, H. H., Jr., J. D. Bredehoeft, and I. S. Papadopulos (1967), Response of a finite-diameter well to an instantaneous charge of water, *Water Resour. Res.*, *3*, 263–269.

d'Astous, A. Y., W. W. Ruland, J. R. G. Bruce, J. A. Cherry, and R. W. Gillham (1989), Fracture effects in the shallow groundwater zone in weathered Sarnia-area clay, *Can. Geotech. J.*, *26*, 43–56.

Davis, E. E., and K. Becker (2001), Using ODP boreholes for studying subseafloor hydrogeology: Results from the first decade of CORK observations, *Geosci. Can.*, *28*(4), 171–178.

Davis, E. E., and K. Becker (2007), On the fidelity of "CORK" borehole hydrologic observatory pressure records, *Sci. Drill.*, *5*, 54–59, doi:10.2204/iodp.sd.5.09.2007.

Davis, E. E., and H. W. Villinger (2006), Transient formation fluid pressures and temperatures in the Costa Rica forearc prism and subducting oceanic basement: CORK monitoring at ODP Sites 1253 and 1255, *Earth Planet. Sci. Lett.*, *245*, 232–244.

Davis, E. E., K. Wang, K. Becker, and R. E. Thomson (2000), Formation-scale hydraulic and mechanical properties of oceanic crust inferred from pore pressure response to periodic seafloor loading, *J. Geophys. Res.*, *105*, 13,423–13,435.

Davis, E. E., K. Wang, R. E. Thomson, K. Becker, and J. F. Cassidy (2001), An episode of seafloor spreading and associated plate deformation inferred from crustal fluid pressure transients, *J. Geophys. Res.*, *106*, 21,953–21,963.

Davis, E. E., K. Becker, R. Dziak, J. Cassidy, K. Wang, and M. Lilley (2004), Hydrological response to a seafloor spreading episode on the Juan de Fuca Ridge, *Nature*, *430*, 335–338.

Davis, E. E., K. Becker, K. Wang, K. Obara, Y. Ito, and M. Kinoshita (2006), A discrete episode of seismic and aseismic deformation of the Nankai Trough subduction zone accretionary prism and incoming Philippine Sea Plate, *Earth Planet. Sci. Lett.*, *242*, 73–84.

Fisher, A. T., and G. Zwart (1997), Packer experiments along the décollement of the Barbados accretionary complex: Measurements of in situ permeability, *Proc. Ocean Drill. Program Sci. Results*, *156*, 199–218.

Fisher, A. T., G. Zwart, and OPD Leg 156 Shipboard Scientific Party (1996), Relation between permeability and effective stress along a plate-boundary fault, Barbados accretionary complex, *Geology*, *24*, 307–310.

Foucher, J. P., P. Henry, and R. Harmegnies (1997), Long-term observations of pressure and temperature in ODP Hole 948D, Barbados accretionary prism, *Proc. Ocean Drill. Program Sci. Results*, *156*, 229–238.

Freeze, R. A., and J. A. Cherry (1979), *Groundwater*, 604 pp., Prentice-Hall, Englewood Cliffs, N. J.

Gamage, K., and E. Screaton (2003), Data report: Permeabilities of Nankai accretionary prism sediments [online], *Proc. Ocean Drill. Program Sci. Results*, *190/196*, 15 pp. (Available at http://www-odp.tamu.edu/publications/190196SR/213/213.htm)

Gamage, K., and E. Screaton (2006), Characterization of excess pore pressures at the toe of the Nankai accretionary complex, Ocean Drilling Program sites 1173, 1174, and 808: Results of one-dimensional modeling, *J. Geophys. Res.*, *111*, B04103, doi:10.1029/2004JB003572.

Gartling, D. K. (1977), Convective heat transfer analysis by the finite element method, *Comput. Methods Appl. Mech. Eng.*, *12*, 365–382.

Gibson, R. E. (1963), An analysis of system flexibility and its effect on time-lag in pore-water pressure measurements, *Geotechnique*, *13*(1), 1–11.

Hsieh, P. A., J. D. Bredehoeft, and J. M. Farr (1987), Determination of aquifer transmissivity from Earth tide analysis, *Water Resour. Res.*, *23*, 1824–1832.

Mikada, H., K. Becker, J. C. Moore, A. Klaus, and Shipboard Scientific Party (2002), *Proceedings of the Ocean Drilling Program Initial Reports*, vol. 196, Ocean Drill. Program, College Station, Tex.

Mikada, H., M. Kinoshita, K. Becker, E. Davis, R. Meldrum, and Shipboard Scientific Party (2003), Hydrological and geothermal studies around Nankai Trough (KR02-10 Nankai Trough Cruise Report), *JAMSTEC J. Deep Sea Res.*, *22*, 125–171.

Moore, G. F., A. Taira, A. Klaus, and Shipboard Scientific Party (2001), *Proceedings of the Ocean Drilling Program Initial Reports*, vol. 190, Ocean Drill. Program, College Station, Tex.

Neuzil, C. E. (1982), On conducting the modified "slug" test in tight formations, *Water Resour. Res.*, *18*, 439–441.

Neuzil, C. E., C. Cooley, S. E. Silliman, J. D. Bredehoeft, and P. A. Hsieh (1981), A transient laboratory method for determining the hydraulic properties of 'tight' rocks, II, Application,, *Int. J. Rock Mech. Min. Sci.*, *18*(3), 253–258.

Papadopulos, S. S., J. D. Bredehoeft, and H. H. Cooper (1973), On the analysis of slug test data, *Water Resour. Res.*, *9*, 1087–1089.

Rojstaczer, S., and F. Riley (1990), Response of the water level in a well to Earth tides and atmospheric loading under unconfined conditions, *Water Resour. Res.*, *26*, 1803–1817.

Sageev, A. (1986), Slug test analysis, *Water Resour. Res.*, *22*, 1323–1333.

Sawyer, A. H. (2007), Response of submarine hydrologic monitoring instruments to formation pressure changes: Theory and application to Nankai ACORKs, M. S. thesis, Pa. State Univ., University Park.

Screaton, E., B. Carson, E. Davis, and K. Becker (2000), Permeability of a decollement zone: Results from a two-well experiment in the Barbados accretionary complex, *J. Geophys. Res.*, *105*, 21,403–21,410.

Taira, A., I. Hill, J. V. Firth, and Shipboard Scientific Party (1991), *Proceedings of the Ocean Drilling Program Initial Reports*, vol. 131, Ocean Drill. Program, College Station, Tex.

van der Kamp, G., and J. E. Gale (1983), Theory of Earth tide and barometric effects in porous formations with compressible grains, *Water Resour. Res.*, *19*, 538–544.

Wang, K., and E. Davis (1996), Theory for the propagation of tidally influenced pore pressure variations in layered subseafloor formations, *J. Geophys. Res.*, *101*, 11,483–11,495.

Wang, K., E. Davis, and G. van der Kamp (1998), Theory for the effects of free gas in subsea formations on tidal pore pressure variations and seafloor displacements, *J. Geophys. Res.*, *103*, 12,339–12,353.

Yang, Y., and A. C. Aplin (2007), Permeability and petrophysical properties of 30 natural mudstones, *J. Geophys. Res.*, *112*, B03206, doi:10.1029/2005JB004243.

D. Elsworth, Department of Energy and Mineral Engineering, Pennsylvania State University, University Park, PA 16802, USA.

P. Flemings and A. H. Sawyer, Department of Geosciences, University of Texas at Austin, 1 University Station C1100, Austin, TX 78712, USA.(asawyer@mail.utexas.edu)

M. Kinoshita, Institute for Research on Earth Evolution, Japan Agency for Marine-Earth Science and Technology, 2-15 Natsushima-cho, Yokosuka, Kanagawa 237-0061, Japan.